https://doi.org/10.5194/egusphere-2026-1058
Preprint. Discussion started: 6 March 2026

Impacts of Cascading Check Dams on Sediment Yield in the Middle Yellow River Basin: Insights from 50 Years of Grid-cell-level Simulation

Yanzhang Huang[1,2], Guangyao Gao[1,2,4,5,*], Lishan Ran[3], Yue Wang[1,2], Mingguo Zheng[6]

[1]State Key Laboratory of Regional and Urban Ecology, Research Center for Eco-Environmental Sciences, Chinese Academy of Sciences, Beijing 100085, China
[2]University of Chinese Academy of Sciences, Beijing 100049, China
[3]Department of Geography, The University of Hong Kong, Hong Kong 999077, China
[4]National Observation and Research Station of Earth Critical Zone on the Loess Plateau in Shaanxi, Xi'an, China
[5]Shaanxi Yan'an Forest Ecosystem Observation and Research Station, Beijing 100085, China
[6]Guangdong Key Laboratory of Integrated Agro-environmental Pollution Control and Management, Institute of Eco-environmental and Soil Sciences, Guangdong Academy of Sciences, Guangzhou 510650, China

Correspondence to: Guangyao Gao (gygao@rcees.ac.cn)

Abstract. Check dams, globally built for controlling soil erosion, form complex cascading systems that pose significant challenges for assessing spatiotemporal dynamics of sediment yield (SY) at large basin scale. This study proposed an integrative framework combining dynamic sediment trapping efficiency of cascading check dams with the Revised Universal Soil Loss Equation (RUSLE), index of connectivity (IC), and sediment delivery ratio (SDR). This model was applied to evaluate grid-cell-based distribution of SY and sediment trapped by check dams during 1970–2020 in the middle Yellow River Basin (with over 47000 check dams). The Nash-Sutcliffe efficiency of proposed model increased to 0.71 compared to model ignoring sediment trapping of check dams (0.59). Check dams reduced the multi-year average SY by 50.01% in dam-controlled areas. Totally 3.84×10^9 t of sediment was trapped over the 50 years, constituting 41.49% of designed storage capacity. The sediment reduction contribution by check dams (SRC_{dam}) exhibited considerable spatial heterogeneity, ranging from 73.9% to 0.9% among sub-basins, and the proportion of accumulated sediment to storage capacity of check dams (SAR_{dam}) varied from 78.1% to 1.1%. The SRC_{dam} increased linearly with check dam density and the share of area they controlled, whereas SAR_{dam} increased logarithmically with SY from upstream of the check dams ($P < 0.001$). A trade-off between SRC_{dam} and SAR_{dam} in some sub-basins indicates that the number of check dams in these basins is insufficient or overmuch. This study provides a practical and data-efficient method for assessing sediment trapping and reduction by cascading check dam systems in large basins, offering valuable insights for improving soil and water conservation strategies in erosion-prone regions.

https://doi.org/10.5194/egusphere-2026-1058
Preprint. Discussion started: 6 March 2026

1 Introduction

Soil erosion, a critical material transport process in terrestrial ecosystems, is a major driver of global soil degradation (Borrelli et al., 2017; Lugato et al., 2018). It severely undermines the achievement of sustainable development goals related to food security (SDG2), water resources (SDG6), and ecosystems (SDG15) (Borrelli et al., 2021, 2023). Mitigating this crisis requires intervening in processes such as slope erosion and fluvial sediment transport to reduce the loss of soil (La Licata et al., 2025). These objectives can be achieved by modifying underlying surface characteristics through measures such as ecological restoration and channel-structure engineering (Maavara et al., 2020; Wang et al., 2025). Quantitatively assessing sediment yield (SY) due to erosion, particularly the interception of sediment by river engineering measures is an indispensable yet challenging component of ecological restoration and river management (Ke and Zhang, 2024).

Among various soil and water conservation measures, damming on river channels is one of the most effective and widely applied methods for trapping sediment and mitigating soil erosion (Esteban Lucas-Borja et al., 2021; Kondolf et al., 2014). These dams are typically defined as transverse structures constructed across riverbeds to control water flow and sediment transport (Abbasi et al., 2019). Numerous check dams have been constructed worldwide, especially in erosion-prone regions with high-density gullies (Sun and Wu, 2023). China has reported the construction of over 50,000 check dams on the Loess Plateau (Zeng et al., 2024). These high-density check dams are built along rivers, forming complex check dam networks (Gao et al., 2024; Li et al., 2022). The spatial interdependence of check dams within watershed networks presents significant challenges for assessing SY reduction. Cascading effects between upstream and downstream structures, where sediment trapping by upper dams directly influences lower ones, constitute a prevalent phenomenon (Pal et al., 2018; do Prado et al., 2024; Sun and Wu, 2023). The complexity of these cascading effects requires the development of computationally efficient approaches to simulate SY within the multi-cascade check dam systems.

Model simulations present a promising alternative for simulating soil erosion and SY (Borrelli et al., 2017). Most studies have evaluated changes in soil erosion by driving models with different input datasets, but without explicitly accounting for the effects of soil and water conservation measures, particularly check dams, on sediment transport (Lan et al., 2023; Schürz et al., 2020; Yin et al., 2025). A few studies have made localized attempts to quantify sediment trapping by check dams. For example, Yang et al. (2024) used a highly complex parametric Geomorphology-Based Ecohydrological Model to evaluate the contribution of check dams to sediment reduction in the Kuye River Basin on the northern Loess Plateau, but simplified the multiple check dams within each sub-basin into a single virtual structure. Sun and Wu (2023) integrated a check-dam module into SWAT; however, their hydrological response unit (HRU)-based semi-distributed modelling framework has deficiencies in positioning and simulation of check dams. Eekhout et al. (2024) assessed the sediment balance contribution of check dams in the Upper Taibilla catchment of Spain by integrating check dam trapping efficiency with an integration of the Morgan-Morgan-Finney soil erosion model into the SPHY hydrological model. This approach, however, requires detailed channel characteristics, which can be difficult to obtain in large catchments (Eekhout et al., 2024). More importantly, existing studies have focused on basin-scale aggregates rather than spatially explicit erosion-delivery-transport processes,

https://doi.org/10.5194/egusphere-2026-1058
Preprint. Discussion started: 6 March 2026

and the grid-cell-level spatial patterns and temporal dynamics of SY reduction by cascading check dams remain poorly understood.

The SY process operates through three routing phases, i.e., soil erosion on hillslope, sediment delivery by overland flow, and sediment transport in channel (Yang et al., 2024), all governed by the overarching concept of sediment connectivity (Fabre et al., 2023). The Revised Universal Soil Loss Equation (RUSLE) can describe soil erosion on the slope (Nistor et al., 2025). DEM-based metrics such as the Index of Connectivity (IC) quantify only structural connectivity (the topographic and landscape configuration that defines potential sediment pathways) (Borselli et al., 2008; Najafi et al., 2021; Shi et al., 2025), whereas the sediment delivery ratio (SDR) provides an empirical proxy for functional connectivity (the realized transfer of sediment driven by rainfall, geography, and vegetation dynamics) (Ke and Zhang, 2024; Shi et al., 2025). Therefore, the integration of RUSLE, IC and SDR, collectively termed the RUSLE-IC-SDR framework, provides a robust methodology for evaluating sediment dynamics across large spatial extents (Abebe et al., 2023; Huang et al., 2024; Vigiak et al., 2012). In highly engineered landscapes, check dams substantially influence connectivity by intercepting and storing sediment, and their influence can be quantified through sediment trapping efficiency (TE) (Fryirs, 2013; Verstraeten and Prosser, 2008). The TE characterizes the capacity of each dam to retain incoming sediment and can be spatially extrapolated as a measure of sediment trapping probability within dam-controlled catchments. Although some studies have combined RUSLE-IC-SDR with TE (Abebe et al., 2023; Zhao et al., 2020), most applications have not explicitly represented their spatiotemporal co-evolution, leaving the spatial distribution and temporal dynamics of sediment transfer and dam-induced retention still insufficiently resolved.

This study proposed an integrative model framework that synergizes the RUSLE-IC-SDR methodology with the check dam sediment trapping module, which systematically accounts for the effects of cascading check dam on sediment yield in large basins. We evaluated spatiotemporal dynamics of grid-cell-based sediment reduction by check dams during 1970-2020 in the middle Yellow River Basin (MYRB). This study aims to: (1) propose a model for describing sediment transport in complex check dam systems at large basin scales; (2) map the spatial distribution of sediment accumulation by check dams and sediment output from the basin; and (3) detect the factors controlling sediment reduction contribution by check dam. The findings will provide scientific information for optimizing the management and layout of soil and water conservation engineering measures within the basin.

2 Materials and Methods

2.1 Study area

The MYRB is located between the Toudaoguai hydrological station and the Huayuankou hydrological station in the Yellow River Basin, China (Fig. 1), covering an area of approximately 34.5×10^4 km^2, with an elevation above sea level ranging from 85 m to 3,917 m. The basin is influenced by a warm temperate monsoon climate. Precipitation is unevenly distributed over space and time, with an average annual rainfall of 320 mm in the northwest to 840 mm in the southwest, mostly

https://doi.org/10.5194/egusphere-2026-1058
Preprint. Discussion started: 6 March 2026

NDVI data every 15 days with a spatial resolution of 8 km from 1982 to 2015 (Pinzon and Tucker, 2014). MOD13Q1 provides NDVI data every 16 days at 250-meter spatial resolution from February 2000 to present. To extend time availability and ensure data comparability, the two NDVI datasets were corrected based on overlapping periods (February 2000 to December 2015) using spatiotemporal stability analysis and statistical downscaling techniques (Huang et al., 2024).

Land use data of five years (1975, 1990, 2000, 2010, and 2020) were obtained from the Institute of Remote Sensing and Digital Earth, Chinese Academy of Sciences, with a spatial resolution of 30 m. The overall accuracy of the land use data was 86% (Wu et al., 2024). We reclassified land use into cropland, forest, grassland, built land, waterbody, and other land use types (Table S2). The 30 m-resolution terrace dataset across China for 2000, 2010, and 2020 was generated using a two-stage random forest classification framework that integrates time-series Landsat imagery with digital elevation model (DEM) data (Zhang et al., 2025). This model utilized the texture features of terraces, achieving a classification accuracy of 91.7%. The vectorized check dam dataset was sourced from YRCC and Zeng et al. (2024). The dataset integrates high-resolution (0.3–1 m) Google Earth imagery from May 2016 to 2020 and an object-based classification method, achieving an overall accuracy of 94.4% (Zeng et al., 2024). This dataset comprises spatial location and storage capacity of check dams. Although the delineation relies on recent imagery, most terraces and check dams in the basin were constructed in the 1970s–1980s, as documented in regional conservation reports.

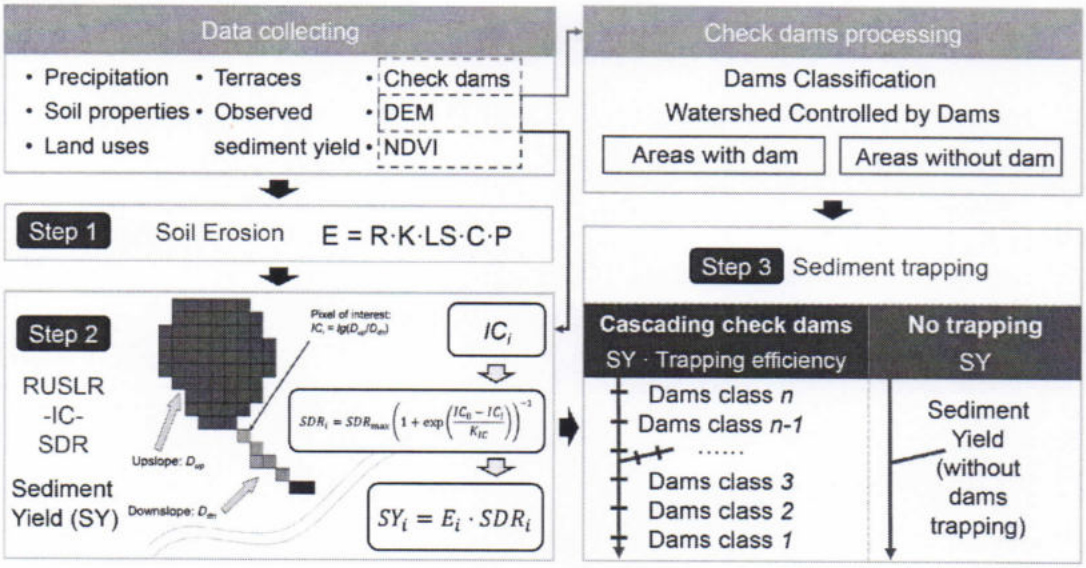

Figure 2. Framework of the integrated model for simulating sediment yield in the basin with cascading check dams. Step 1 denotes the soil erosion module by RUSLE. Step 2 indicates the sediment yield module by "RUSLE-IC-SDR" method. Step 3 represents the sediment trapping module by check dam. IC represents the index of connectivity, and SDR denotes the sediment delivery ratio.

https://doi.org/10.5194/egusphere-2026-1058
Preprint. Discussion started: 6 March 2026

$$IC_i = lg\left(\frac{D_{up}}{D_{dn}}\right) = lg\left(\frac{\overline{WS}\sqrt{A_{up}}}{\sum_i \frac{d_i}{W_i S_i}}\right), \quad (2)$$

$$SDR_i = SDR_{max}\left(1 + e^{\left(\frac{IC_0 - IC_i}{K_{IC}}\right)}\right)^{-1}, \quad (3)$$

where D_{up} and D_{dn} represent the upslope and downslope components of the connectivity, respectively. $\overline{W}$ is the average weighting factor of the upslope contributing area (dimensionless). $\overline{S}$ is the average slope gradient of the upslope contributing area (m m^{-1}). A_{up} is the upslope contributing area (m^2). d_i is the length of the flow path along the ith cell according to the steepest downslope direction (m). W_i is the weighting factor of the ith pixel (dimensionless), and the C factor in RUSLE was usually specified as the weighting factor (Zhao et al., 2020). S_i is the slope gradient of the ith pixel (m m^{-1}). SDR_{max} is the maximum theoretical SDR, which was assumed to be 1 at cell scale. SDR_i is the sediment delivery ratio of the ith pixel. IC_0 and K_{IC} are landscape-independent and landscape-dependent calibration parameters, respectively, which define the shape of the sigmoid function of the SDR-IC relationship (La Licata et al., 2025; Vigiak et al., 2012).

The index of connectivity (IC) was computed using the stand-alone SedInConnect Python scripts (Crema and Cavalli, 2018). Then, the sediment yield (SY, t ha^{-1} yr^{-1}) could be estimated using soil erosion rates and the SDR (Huang et al., 2024):

$$SY_i = E_i \cdot SDR_i, \quad (4)$$

where SY_i (t ha^{-1} yr^{-1}) is the off-site SY of the ith pixel, E_i is the soil erosion rate of the ith pixel.

2.3.3 Sediment trapping module by check dams

The sediment trapping efficiency (TE) of check dams refers to the proportion of incoming sediments that are deposited or captured behind dams. An empirical relationship that relates TE to the effective storage capacity and the watershed area controlled by check dams has been used widely (Verstraeten & Poesen, 2000):

$$TE = 100\left(1 - \frac{1}{1 + 0.0021D\frac{V}{A_{cca}}}\right), \quad (5)$$

where V denotes the remaining storge capacity (m^3) of a check dam, A_{cca} is the contributing catchment area (km^2), and D is a value ranging from 0.046 to 1 (values of D = 0.046, 0.1, and 1.0 can be used for fine, medium, and coarse sediments, respectively) suggested by Verstraeten and Poesen (2000). A value of 0.046 was selected due to the relatively fine loess in the study area (Zhao et al., 2020).

The presence of 47,391 check dams, along with interconnected and parallel check dam systems, posed a significant challenge to accurately calculate the sediment trapping capacity of check dams. To facilitate the acquisition of dam-controlled watershed areas, we utilized the "Feature To Point" tool in ArcGIS 10.2 to generate point for the check dams. Subsequently, the "Snap Pour Point" tool was employed to direct the check dam points within a 100-m distance towards the cells with the highest flow accumulation. A key methodological contribution of this study is the development of a systematic check-dam classification and routing framework that allows sediment delivery and trapping to be computed sequentially

https://doi.org/10.5194/egusphere-2026-1058
Preprint. Discussion started: 6 March 2026

along complex dam cascades without double-counting. (Fig. 3a). A dam assigned to class "*n*" represents a dam for which *n* dams occur along the downstream flow path to the cascade outlet (Fig. 3b); thus, the furthest upstream dam has the highest class number, while the terminal dam has class "1". This classification enables sediment routing to be solved in a strictly upstream-to-downstream order, ensuring that sediment trapped in upstream dams is subtracted before calculating the sediment retained by any downstream dam (Fig. 3c). Compared with the HRU-based identification and conceptualization of check dam networks used by Sun and Wu (2023), our method provides a more efficient and straightforward way to handle large and complex check-dam systems.

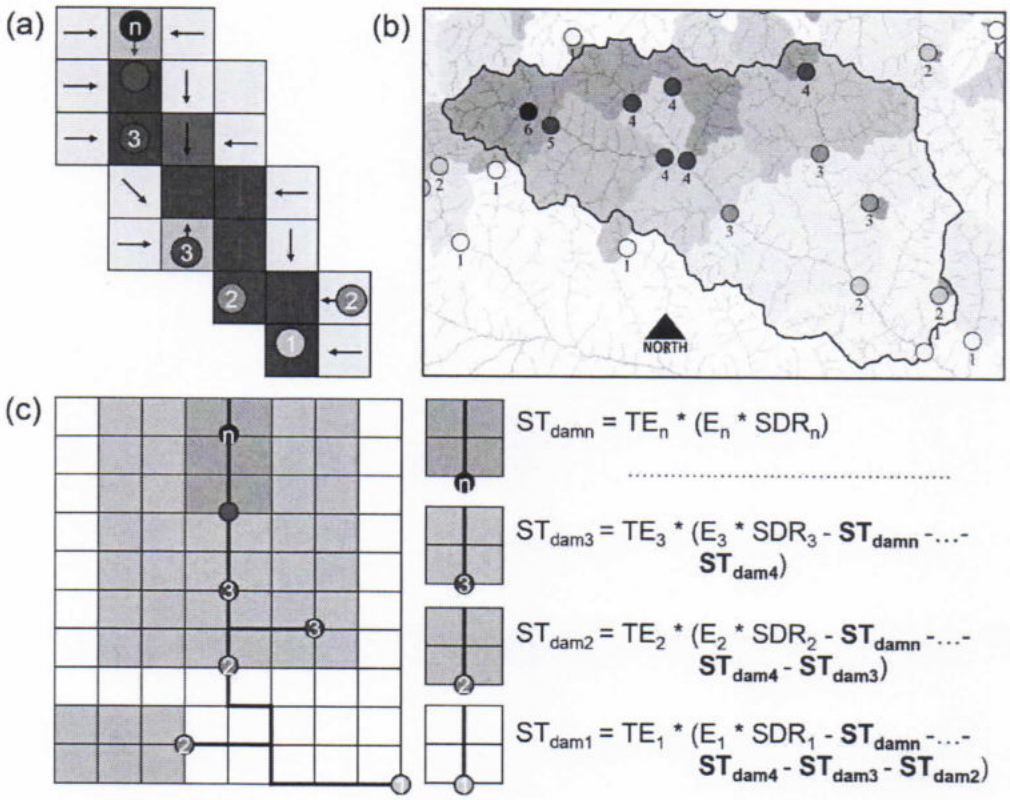

Figure 3. The generalized process and conceptual diagram of sediment trapping by cascading check dam system. (a) An example of check dam classification based on flow direction data. (b) An example of cascading check dam distribution in a catchment. (c) Equations to describe sediment trapping by cascading check dams. ST_{damn}, …, ST_{dam3}, ST_{dam2}, and ST_{dam1} represent sediment trapped in the area controlled by check dam class n, …, 3, 2, and 1, respectively. TE represents the sediment trapping efficiency of the check dams; E and SDR refer to the pixel-based soil erosion rate and sediment delivery ratio, respectively.

https://doi.org/10.5194/egusphere-2026-1058
Preprint. Discussion started: 6 March 2026

To illustrate this procedure, Fig. 3b shows a typical watershed with multiple dams. For a downstream dam (e.g., dam 1), accurate estimation of its trapped sediment requires beginning with the furthest upstream dam (class n) and iteratively subtracting the sediment deposited in all upstream dams (class n, n-1, …, 2), as depicted in Fig. 3c. Algorithmically, this framework was implemented by combining flow direction, flow accumulation, and dam-point geometry in Python to determine the full topological ordering of dams. Once classified, individual dam-controlled watersheds were delineated using the "*arcpy*" package in Python (Fig. 3b), enabling the removal of overlapping contributing areas and preventing the artificial multiplication of TE where dam influence areas intersect. This step is essential because cascading check dams frequently generate overlapping control regions, and failing to separate them can lead to substantial overestimation of trapped sediment (Fig. 3b, c). After establishing the classification system and routing sequence, we implemented annual sediment routing and trapping computations for 1970–2020 using Python with "*multiprocessing*" and "*joblib*" to improve computational efficiency across 47391 dams. Sediment accumulation in each check dam was recorded annually to track long-term storage development. The soil bulk density was set at 1.47 g cm^{-3} in this study, based on an average of 60 samples from six profiles (0–12 m) by Fang et al. (2023) on the Loess Plateau.

2.4 Parameter calibration and simulation analysis

The conversion from IC to SDR requires calibrating the parameters IC_0 and K_{IC}. Due to variations in sub-basin characteristics such as topography, soil, and climate (Hao et al., 2022), the optimal combinations of IC_0 and K_{IC} differ across sub-basins. In this study, we conducted individual parameter calibration for 17 sub-basins controlled by hydrological stations. Initially, 70 combinations of IC_0 and K_{IC} were tested, with IC_0 ranging from -7 to -1 (in steps of 1) and K_{IC} from 0.5 to 5 (in steps of 0.5). Each parameter set was applied to the proposed integrated SY model in each sub-basin. This process was repeated for all the 70 combinations, yielding SY values with accounting for trapping of check dams. The observed and simulated SY were compared to evaluate the model's predictive capability using the Nash-Sutcliffe efficiency coefficient (*NSE*) (Huang et al., 2024). If the optimal parameter combination fell outside the initial range, the parameter steps were adjusted based on the trend of *NSE* variation until the optimal combination was identified. For the remaining areas outside these 17 sub-basins, we used the average of the optimal parameters of nearby sub-basins to calculate SDR, which is used to complete the SY estimation for the entire MYRB.

Previous applications of the traditional RUSLE-IC-SDR framework do not explicitly account for the sediment trapping of the dams (Lan et al., 2023; Schürz et al., 2020; Yin et al., 2025). Building on this context, the key focus of our study was the explicit incorporation of TE-based check-dam trapping, which represents sediment interception and storage within each dam along cascading dam systems. To evaluate the impact of check dams trapping within the RUSLE-IC-SDR framework, we compared two model configurations. The first configuration activates the full TE-based trapping scheme, while the second follows the traditional RUSLE-IC-SDR setup in which sediment is routed through the landscape without sediment trapping by check dams. The combinations of IC_0 and K_{IC} in this scenario remained identical to that in the actual check dam-regulated scenario. This design ensures that the only difference between the two simulations is whether check-dam trapping is

https://doi.org/10.5194/egusphere-2026-1058
Preprint. Discussion started: 6 March 2026

represented. The resulting sediment yields are denoted as SY_{Trap} (with sediment trapping) and SY_{noTrap} (without sediment trapping), and the sediment reduction contribution by check dams (SRC_{dam}) was computed as:

$$SRC_{dam} = \frac{SY_{noTrap} - SY_{Trap}}{SY_{Trap}} \times 100\% \quad (6)$$

3 Results

3.1 Performance of integrated model considering cascading check dams

The check dams primarily distributed in the central part of the MYRB, forming highly complex cascading systems (Fig. 4). The area controlled by check dams is 4.68 × 10^4 km^2, accounting for 13.55% of the MYRB. The total designed storage capacity of all check dams is 6.36 × 10^9 m^3, predominantly comprising small dams (< 10 × 10^4 m^3), which account for 68.0% of the total number (Fig. 4a). There was 68.78% (n = 32,595) of the check dams within a cascading system. Within these systems, ⩾6-tier check dams constitute 16.65% (n = 7,892) of the total count, while a subset of 0.56% (n = 265) exhibit exceptionally high class (16–27 tiers), indicating 16–27 sequentially constructed check dams along river channels from upstream to downstream (Fig. 4b).

The proposed model framework considered the effects of cascading check dams on SY. The optimal combinations of IC_0 and K_{IC} in the model varied across sub-basins (Fig. S1). Our analysis demonstrates that models incorporating check dam sediment trapping exhibit superior model performance compared to counterparts excluding check dams (Fig. 5). Model performance validation using observed SY from 17 hydrological stations in the MYRB showed that incorporating the sediment trapping of check dams could improve the NSE to 0.713 (R^2 = 0.71) (Fig. 5a), representing a 20.0% improvement compared to the traditional model (NSE = 0.594, R^2 = 0.72) (Fig. 5b).

https://doi.org/10.5194/egusphere-2026-1058
Preprint. Discussion started: 6 March 2026

During 1970–2001, the multi-year average SY in MYRB was 17.41 ± 3.61 t ha^{-1} yr^{-1}, showing no significant changing trend (P = 0.184) (Fig. 7). After 2002, the average SY decreased to 11.89 ± 3.93 t ha^{-1} yr^{-1}, representing a 31.71% reduction compared to 1970-2001, with a statistically significant downward trend during 2002-2020 (P < 0.001) (Fig. 7). Furthermore, the difference in SY between scenarios with and without sediment trapping by check dams has been gradually narrowed, decreasing from 14.42% during 1970–2001 to 7.45% in the post-2001 period (Fig. 7).

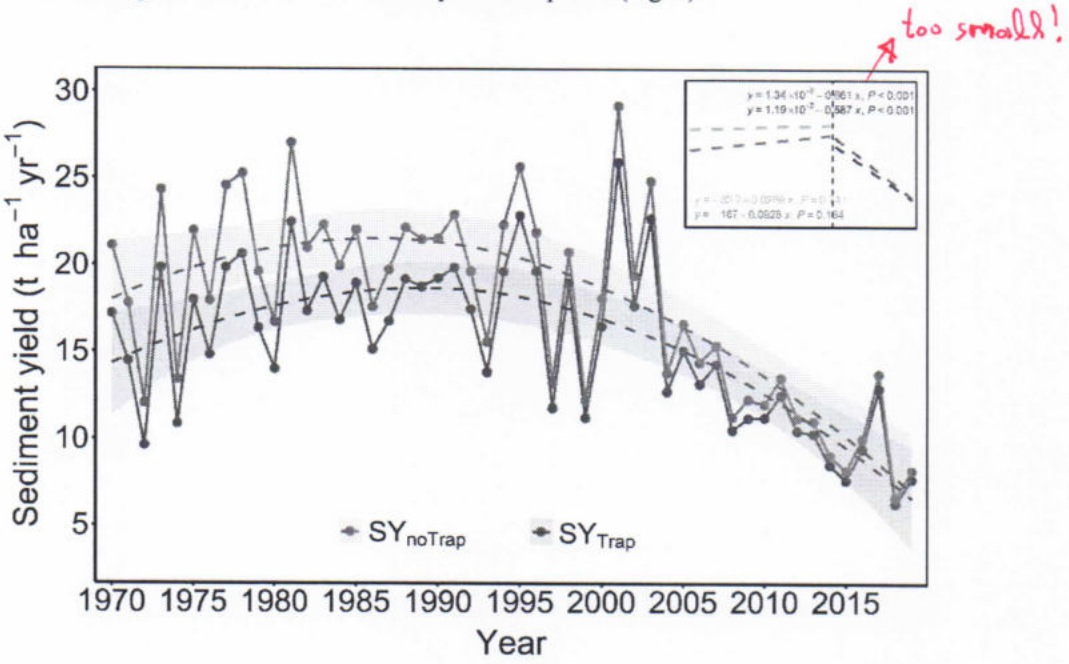

Figure 7. Interannual variations in average sediment yield (SY) with (SY$_{Trap}$) and without (SY$_{noTrap}$) sediment trapping by check dams during 1970–2020 in the middle Yellow River Basin. The dashed line represents a fitted curve, with the shaded area indicating the 95% confidence interval. The inset in the upper right displays the linear regression trend of SY before and after 2001.

3.3 Dynamics of sediment reduction and trapping by check dams

In the MYRB, the overall trend in sediment reduction contribution by check dams (SRC$_{dam}$) showed a gradual decline, with a 50-year average value of 13.68 ± 5.98% (Fig. 8). In the first decade (1970–1979), the SRC$_{dam}$ remained above 20%. During 1980–2001, the SRC$_{dam}$ was 14.47 ± 3.45%, whereas after 2002, it significantly declined to 7.74 ± 1.39% (P < 0.001) (Fig. 8). The SRC$_{dam}$ varied widely across sub-basins, ranging from 1.01% in *Fen River* basin to 110.75% in *Jialu River* basin in the first decade (Fig. S8). During 1980–2001, SRC$_{dam}$ in sub-basins ranged from 0.92% (*Fen River* basin) to 78.05% (*Jialu River* basin). After 2002, the range of SRC$_{dam}$ narrowed to 0.94% (*Fen River* basin)–59.97% (*Fenchuan River* basin).

https://doi.org/10.5194/egusphere-2026-1058
Preprint. Discussion started: 6 March 2026

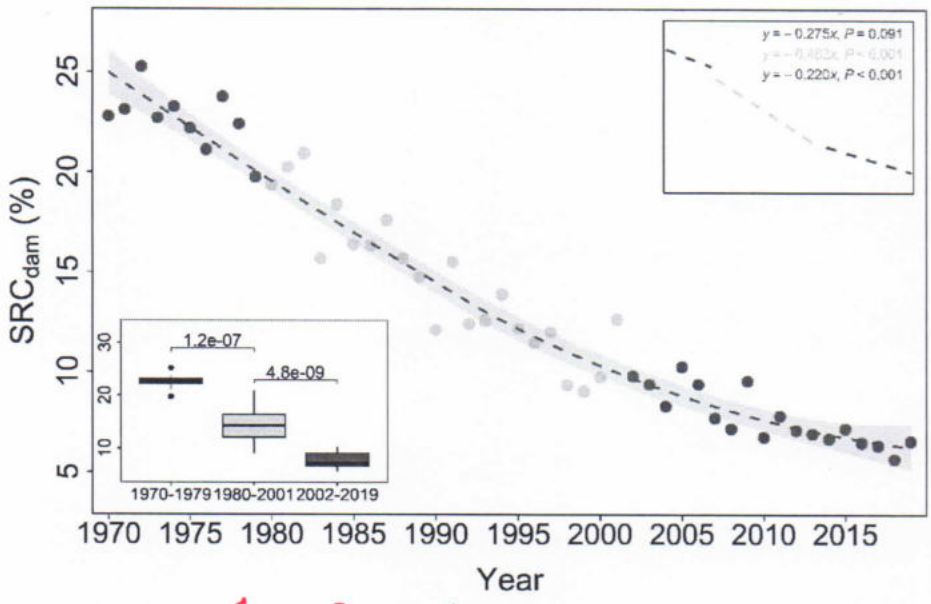

Figure 8. Interannual variations in the sediment reduction contribution of check dam (SRC_{dam}) in the middle Yellow River Basin. The inset in the lower left represents the average SRC_{dam} during the 1970–1979, 1980–2001, and 2002–2020. The shaded area indicates the 95% confidence interval.

The accumulated sediment trapped by all check dams in the MYRB over the past 50 years was 3.84×10^9 t, occupying 41.49% of the total designed storage capacity (Fig. 9). During the first decade, sediment accumulation rates in check dams were highest, averaging 126.24×10^6 t yr^{-1}, accounting for 13.62% of the total storage capacity (Fig. 9). Between 1980–2001 and post-2001, the average sediment accumulation rates decreased to 90.29×10^6 t yr^{-1} and 33.03×10^6 t yr^{-1}, respectively. Accumulated sediment during these two periods represented 21.44% and 6.42% of the total storage capacity, respectively (Fig. 9).

In the first decade (1970–1979), check dams were filled rapidly, with only 27.13% of check dams retaining more than 95% of their storage capacity, while 8.30% had already lost over 90%. By 2001, sediment accumulation further reduced storage capacity, with just 9.48% of check dams maintaining over 95% capacity and 29.92% experiencing losses of exceeding 90% capacity (Fig. 9). Until 2020, 55.08% of the check dams lost more than 50% of their storage capacity due to sediment deposition (Fig. 9). Among these, 37.47% of the check dams lost over 90% of their storage capacity, and only 7.43% of the check dams accumulated less than 5% capacity (Fig. 9).

The degree of sediment accumulation in check dams varied across different sub-basins in the MYRB (Fig. S9). Over the past 50 years, the total sediment accumulation in check dams across the 17 sub-basins ranged from 1.06% (*Fen River* basin) to 78.12% (*Huangfuchuan River* basin) of the total storage capacity (coefficient of variation, CV = 63.89%) (Fig. S9). Additionally, within these sub-basins, 0.54% (*Qingjian River* basin) to 87.94% (*Fen River* basin) (CV = 135.55%) of check

https://doi.org/10.5194/egusphere-2026-1058
Preprint. Discussion started: 6 March 2026

dams experienced less than 5% losses of storage capacity, while 2.78% (*Zhujiachuan River* basin) to 76.39% (*Kuye River* basin) (CV = 75.12%) of check dams suffered exceeding 90% storage capacity losses (Fig. S9).

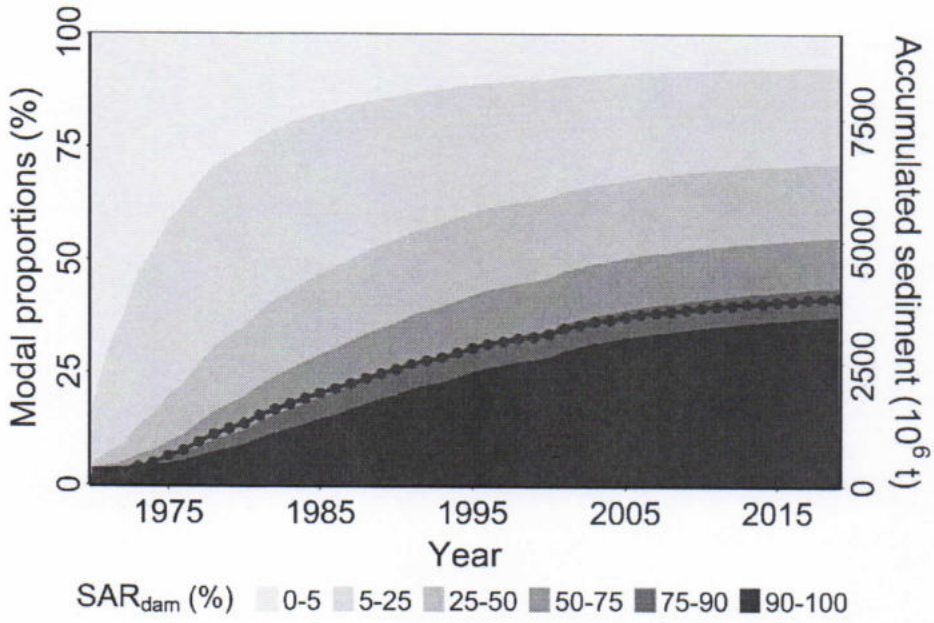

Figure 9. Modal proportions of check dams characterized by different proportions of accumulated sediment relative to total storage capacity (SAR_{dam}) (colored fill), alongside annual changes in accumulated sediment in check dams (purple dotted line) in the middle Yellow River Basin.

4 Discussion

4.1 Factors controlling sediment reduction and trapping by check dams

The temporal dynamics of SRC_{dam} were influenced by check dam characteristics (such as number, density, controlled area, and storage capacity) and sediment yielding status (such as the magnitude of SY and its spatial distribution) (Bai et al., 2020; Sun and Wu, 2023). Prior to the implementation of vegetation restoration projects, the vegetation coverage was only 25.08% during 1980s in the MYRB (Zhang et al., 2022), and severe soil erosion occurred in the basin (Fig. S2). The resulting high SY, combined with the initially high effective storage capacity of newly check dams, jointly contributed to a high SRC_{dam} (Verstraeten and Poesen, 2000). As sediment accumulates in check dams, their effective storage capacity diminishes, resulting in a decreasing TE (Fig. S6b) and SRC_{dam} (Fig. 8). With the implementation of "Grain for Green" program (GGP) since 2000, the vegetation coverage has increased to 58.68% recently (Zhang et al., 2022). The improved vegetation has significantly curbed hillslope soil erosion by intercepting rainfall, enhancing infiltration, and consolidating the soil (Ebabu et

https://doi.org/10.5194/egusphere-2026-1058
Preprint. Discussion started: 6 March 2026

al., 2022). As a result, SY has markedly decreased, leading to a more stable and further lower SRC_{dam} over time (Sun et al., 2020).

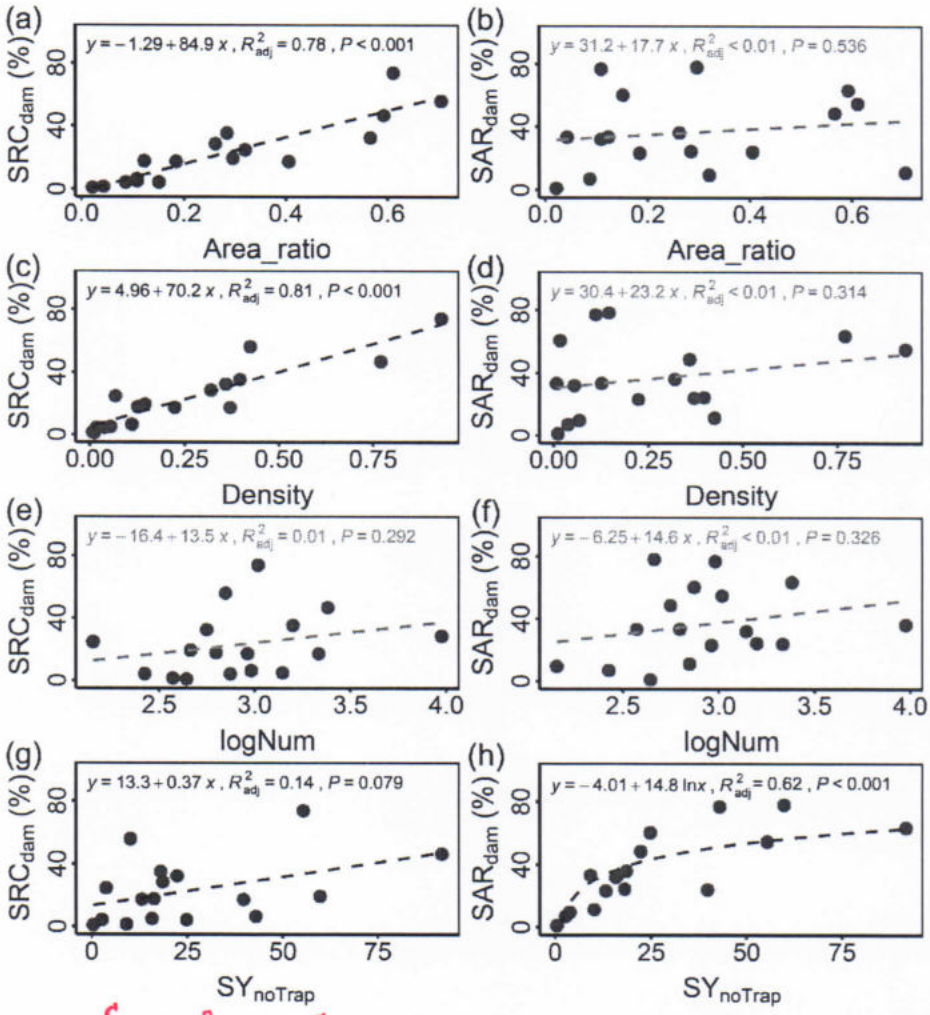

Figure 10. Correlations of sediment reduction contribution of check dams (SRC_{dam}) and proportion of accumulated sediment relative to total storage capacity (SAR_{dam}) with the proportion of area controlled by check dams to the total basin area (Area_ratio) (a and b), check dam density (Density) (c and d), logarithm of the number of check dams (logNum) (e and f), and average sediment yield without sediment trapping by check dams (SY_{noTrap}) in sub-basins (g and h).

The SRC_{dam} and proportion of accumulated sediment to storage capacity of check dams (SAR_{dam}) differed substantially among 17 sub-basins (Fig. S8). Figure 10 shows the relationships of SRC_{dam} and SAR_{dam} with check dam related factors (number of check dams, check dam density, the proportion of the watershed area controlled by check dams to the total basin

https://doi.org/10.5194/egusphere-2026-1058
Preprint. Discussion started: 6 March 2026

Check dams are well known to rapidly halt channel incision and stabilize gully beds, yet these geomorphic adjustments are not directly captured by the current model structure (Piton et al., 2017). Future research should focus on incorporating gully erosion, bank erosion, and bed incision modules to better represent the full suite of geomorphic processes influenced by check dams (He et al., 2026). In addition, considering the increasing frequency of extreme climatic events, future research should focus on understanding how extreme rainfall events and associated geological hazards, such as debris flows, influence sediment trapped by check dams (Chen et al., 2025). Such work is essential to predict and prevent sudden dam failures, which could significantly compromise flood control and sediment retention functions (Esteban Lucas-Borja et al., 2021). Considering the growing interest in carbon burial in dammed sediments, coupling sediment-retention modelling with carbon-dynamics processes is another important direction (Yao et al., 2022). Despite the above limitations, the proposed framework substantially improves the ability to diagnose sediment dynamics in large, highly engineered basins and provides a foundation for more comprehensive modelling of cascading check-dam networks.

5 Conclusions

In this study, we proposed a framework coupling RUSLE-IC-SDR and TE, to simulate the spatial distribution of SY over past 50 years in the MYRB under the influences of complex check dam networks. The findings show that the check dams reduced the multi-year average SY by 50.01% in dam-controlled areas. The SY reduction contribution by check dams exhibited considerable spatial heterogeneity, ranging from 73.9% to 0.9% among sub-basins. Over the study period, check dams retained total sediment of 3.84×10^9 t, filling 41.49% of their designed storage capacity, with the accumulation rate decreasing considerably from 126.14×10^6 t yr^{-1} in the initial stage to 33.03×10^6 t yr^{-1} in recent decade. The SY reduction contribution by check dams was more strongly associated with dam-specific parameters, such as check dam density and the proportion of area controlled by check dams to the total basin area, whereas the sediment accumulation efficiency was primarily affected by the sediment yield from upstream of the check dams. Further, there was evident trade-off between SY reduction contribution and sediment accumulation efficiency of check dams in some sub-basins, indicating that the number of check dams in these basins is insufficient or overmuch. Overall, this study provides a practical and data-efficient method for assessing sediment trapping and reduction by cascading check dam systems in large basin, offering valuable insights for improving soil and water conservation strategies in erosion-prone regions.

Code and data availability

The observed sediment yield, land use, simulated sediment yield, and codes related to this research are openly available on figshare (Huang et al., 2025) at https://doi.org/10.6084/m9.figshare.29400029. The high-quality gridded precipitation dataset (called CHM_PRE) is available on figshare (Han et al., 2022) at https://doi.org/10.6084/m9.figshare.21432123.v4. The SoilGrids dataset can be downloaded from ISRIC (2021) at https://soilgrids.org. SRTM DEM can be downloaded from

https://doi.org/10.5194/egusphere-2026-1058
Preprint. Discussion started: 6 March 2026

van der Knijff, J. M., Jones, R. J. A., and Montanarella, L.: Soil erosion risk assessment in Europe, 2000.

Kondolf, G. M., Gao, Y., Annandale, G. W., Morris, G. L., Jiang, E., Zhang, J., Cao, Y., Carling, P., Fu, K., Guo, Q., Hotchkiss, R., Peteuil, C., Sumi, T., Wang, H., Wang, Z., Wei, Z., Wu, B., Wu, C., and Yang, C. T.: Sustainable sediment management in reservoirs and regulated rivers: Experiences from five continents, Earth's Futur., 2, 256–280, https://doi.org/10.1002/2013ef000184, 2014.

Lan, X., Liu, Z., Yang, T., Cheng, L., Wang, X., Wei, W., Ge, Y., Chen, X., Lin, K., Zhao, T., Zhang, X., and Zhou, G.: Land-Use Intensity Reversed the Role of Cropland in Ecological Restoration Over the World's Most Severe Soil Erosion Region, Earth's Futur., 11, e2022EF003388, https://doi.org/10.1029/2022EF003388, 2023.

Li, P., Chen, J., Zhao, G., Holden, J., Liu, B., Chan, F. K. S., Hu, J., Wu, P., and Mu, X.: Determining the drivers and rates of soil erosion on the Loess Plateau since 1901, Sci. Total Environ., 823, 153674, https://doi.org/10.1016/j.scitotenv.2022.153674, 2022a.

Li, Z., Li, P., Yu, Y., Shi, P., and Piton, G.: Check Dam Construction for Sustainable Watershed Management and Planning, edited by: Li, Z., Li, P., Yu, Y., Shi, P., and Piton, G., Wiley, https://doi.org/10.1002/9781119742449, 2022b.

La Licata, M., Bosino, A., Sadeghi, S. H., De Amicis, M., Mandarino, A., Terret, A., and Maerker, M.: HOTSED: A new integrated model for assessing potential hotspots of sediment sources and related sediment dynamics at watershed scale, Int. Soil Water Conserv. Res., 13, 80–101, https://doi.org/10.1016/j.iswcr.2024.06.002, 2025.

Esteban Lucas-Borja, E., Piton, G., Yu, Y., Castillo, C., and Antonio Zema, D.: Check dams worldwide: Objectives, functions, effectiveness and undesired effects, Catena, 204, 105390, https://doi.org/10.1016/j.catena.2021.105390, 2021.

Lugato, E., Smith, P., Borrelli, P., Panagos, P., Ballabio, C., Orgiazzi, A., Fernandez-Ugalde, O., Montanarella, L., and Jones, A.: Soil erosion is unlikely to drive a future carbon sink in Europe, Sci. Adv., 4, eaau3523, https://doi.org/10.1126/sciadv.aau3523, 2018.

Maavara, T., Chen, Q., Van Meter, K., Brown, L. E., Zhang, J., Ni, J., and Zarfl, C.: River dam impacts on biogeochemical cycling, Nat. Rev. Earth Environ., 1, 103–116, https://doi.org/10.1038/s43017-019-0019-0, 2020.

Najafi, S., Dragovich, D., Heckmann, T., and Sadeghi, S. H.: Sediment connectivity concepts and approaches, Catena, 196, 104880, https://doi.org/10.1016/j.catena.2020.104880, 2021.

NASA Jet Propulsion Laboratory.: (2013). NASA Shuttle Radar Topography Mission Global 1 arc second [Data set], https://doi.org/10.5067/MEASURES/SRTM/SRTMGL1.003, 2013

Nistor, C., Săvulescu, I., Ioana-Toroimac, G., and Carablaisă, S.: Exploring soil erosion and reservoir sedimentation through the RUSLE model and bathymetric survey, Int. Soil Water Conserv. Res., 13, 235–247, https://doi.org/10.1016/j.iswcr.2024.10.005, 2025.

NOAA.: Global GIMMS NDVI3g v1 dataset (1981-2015) [Data set], https://data.tpdc.ac.cn/en/data/9775f2b4-7370-4e5e-a537-3482c9a83d88, 2018.

Pal, D., Galelli, S., Tang, H., and Ran, Q.: Toward improved design of check dam systems: A case study in the Loess Plateau, China, J. Hydrol., 559, 762–773, https://doi.org/10.1016/j.jhydrol.2018.02.051, 2018.